UCLA
UCLA Previously Published Works

Title

THz and mm-Wave Sensing of Corneal Tissue Water Content: Electromagnetic Modeling and Analysis

Permalink

https://escholarship.org/uc/item/8sf622tn

Journal

IEEE Transactions on Terahertz Science and Technology, 5(2)

ISSN

2156-342X

Authors

Taylor, Zachary D
Garritano, James
Sung, Shijun
et al.

Publication Date

2015-03-01

DOI

10.1109/tthz.2015.2392619

Peer reviewed

THz and mm-Wave Sensing of Corneal Tissue Water Content: *In Vivo* Sensing and Imaging Results

Zachary D. Taylor [Member, IEEE],
Department of Bioengineering, University of California (UCLA), Los Angeles, CA 90095 USA, and also with the Center for Advanced Surgical and Interventional Technology (CASIT), University of California (UCLA), Los Angeles, CA 90095 USA

James Garritano,
Department of Bioengineering, University of California (UCLA), Los Angeles, CA 90095 USA, and also with the Center for Advanced Surgical and Interventional Technology (CASIT), University of California (UCLA), Los Angeles, CA 90095 USA

Shijun Sung [Member, IEEE],
Department of Electrical Engineering, University of California (UCLA), Los Angeles, CA 90095 USA

Neha Bajwa,
Department of Bioengineering, University of California (UCLA), Los Angeles, CA 90095 USA, and also with the Center for Advanced Surgical and Interventional Technology (CASIT), University of California (UCLA), Los Angeles, CA 90095 USA

David B. Bennett [Member, IEEE],
Department of Electrical Engineering, University of California (UCLA), Los Angeles, CA 90095 USA. He is now with Fitbit, San Francisco, CA 94105 USA

Bryan Nowroozi,
Department of Bioengineering, University of California (UCLA), Los Angeles, CA 90095 USA, and also with the Center for Advanced Surgical and Interventional Technology (CASIT), University of California (UCLA), Los Angeles, CA 90095 USA. He is now with Mimeo Labs Inc, Santa Monica, CA 90404 USA

Priyamvada Tewari,
Department of Bioengineering, University of California (UCLA), Los Angeles, CA 90095 USA, and also with the Center for Advanced Surgical and Interventional Technology (CASIT), University of California (UCLA), Los Angeles, CA 90095 USA. She is now with Elsevier Life Science solutions, San Francisco, CA 94105 USA

James W. Sayre,
Department of Biostatistics, University of California (UCLA), Los Angeles, CA 90095 USA

Jean-Pierre Hubschman,
Department of Ophthalmology, University of California (UCLA), Los Angeles, CA 90095 USA

Sophie X. Deng,

Department of Ophthalmology, University of California (UCLA), Los Angeles, CA 90095 USA

Elliott R. Brown [Fellow, IEEE], and
Department. of Electrical Engineering, Wright State University, Dayton, OH 45435 USA

Warren S. Grundfest [Member, IEEE]
Department of Bioengineering, University of California (UCLA), Los Angeles, CA 90095 USA, and also with the Center for Advanced Surgical and Interventional Technology (CASIT), University of California (UCLA), Los Angeles, CA 90095 USA

Zachary D. Taylor: zdeis@seas.ucla.edu

Abstract

A pulsed terahertz (THz) imaging system and millimeter-wave reflectometer were used to acquire images and point measurements, respectively, of five rabbit cornea *in vivo*. These imaging results are the first ever produced of *in vivo* cornea. A modified version of a standard protocol using a gentle stream of air and a Mylar window was employed to slightly dehydrate healthy cornea. The sensor data and companion central corneal thickness (CCT) measurements were acquired every 10–15 min over the course of two hours using ultrasound pachymmetry.. Statistically significant positive correlations were established between CCT measurements and millimeter wave reflectivity. Local shifts in reflectivity contrast were observed in the THz imagery; however, the THz reflectivity did not display a significant correlation with thickness in the region probed by the 100 GHz and CCT measurements. This is explained in part by a thickness sensitivity at least $10\times$ higher in the mm-wave than the THz systems. Stratified media and effective media modeling suggest that the protocol perturbed the thickness and not the corneal tissue water content (CTWC). To further explore possible etalon effects, an additional rabbit was euthanized and millimeter wave measurements were obtained during death induced edema. These observations represent the first time that the uncoupled sensing of CTWC and CCT have been achieved *in vivo*.

Index Terms

Biological and medical imaging; clinical instruments; medical diagnostics; tissue water content interactions

I. Introduction

Terahertz (THz) tissue water content (TWC) sensing continues to gain traction in medical imaging, driven largely by active, stand-off sensing systems having THz frequency illumination that enables spatio-temporal mapping of water gradients near the surface of physiologic tissues [1], [2]. The easily accessible tissue of the cornea offers a unique opportunity for TWC mapping given its low physiologic variation and homogenous composition when compared to other tissue systems in the human body [3]–[5].

In a companion paper, we address a theoretical 1D wave model and simulation study of the THz frequency properties of the cornea [6]. This work emphasizes the properties of the lossy etalon effect that arises from the cornea lying in between the aqueous humor and the cornea presents to external radiation, and elucidates the THz electromagnetic properties under

simultaneous perturbations of corneal tissue water content (CTWC) and central corneal thickness (CCT). Three candidate tissue water content (TWC) gradient types were explored: (1) pinned back where the CTWC changes occur primarily at the posterior surface, (2) pinned front where the TWC changes occur primarily at the anterior surface close to the aqueous humor, and (3) global where the CTWC modulation occurs evenly throughout the entire thickness of the cornea. The quantity $\overline{\mathrm{CTWC}}$ was also introduced which represents the CTWC averaged over the entire thickness to allow gradients types to be compared on a common axis.

The expected reflectivities of these gradient types were computed using candidate system spectral transfer functions with center frequencies of 100 GHz and 525 GHz, and bandwidths of Q = 5 and Q = 50. The results discussed an anti-correlation between reflectivity and CTWC in the pinned front gradient type and identified an inherent ambiguity in CTWC sensing where numerous $\mathrm{CCT}{-}\overline{\mathrm{CTWC}}$ pairs resulted in the same reflectivity. The key result of these simulations was the confirmation of the thin film like behavior of cornea when probed with millimeter wave and THz frequency illumination, suggesting that simultaneous measurement of thickness and CTWC gradients through the acquisition of an ensemble of reflectivities at different frequencies is possible. Furthermore, due to the low physiologic variation of corneal structure, a strong set of *a priori* knowledge on corneal geometry precludes the need for phase sensitive measurements and may even allow for depth resolved measurements of the axial CTWC distribution.

In this paper we report on the use of THz imaging and millimeter-wave reflectometry in the generation of spatially and temporally resolved reflectivity maps of cornea. Contrast generation is explored in rabbit models and the first ever *in vivo* images of corneal tissue are presented. Statistically significant correlations were established between increasing millimeter wave reflectivities and increasing central corneal thickness (CCT) measurements. Conversely, correlations between CCT measurements and THz reflectivity were weak, as the THz data showed both increases and decreases in THz reflectivity as the corneal thickness increased. Electromagnetic modeling suggests that the protocol changed the thickness of the cornea in each animal model while leaving the TWC relatively unchanged, and that the signal variation (or lack thereof) was due primarily to etalon effects. To further explore this effect an additional rabbit was prepared with the same protocol, euthanized, and the reflectivity was observed to increase as the corneal thickness increased, then decrease. Animal death is known to correlate with simultaneous increases in CTWC and CCT [7] and modeling of these changes predicted the non-monotonic behavior.

This data represents the first quantitative *in vivo* demonstration of the decoupled sensing of CTWC and CCT and demonstrates the potential of THz CTWC imaging.

II. Standoff Tissue Water Content Contrast Generation Systems

Two CTWC sensing systems were designed and constructed for the rabbit trial (Section IV); one narrow band system operating at 100 GHz with a *Q* of ~50 (millimeter wave system) and one broad band system operating at a center frequency of ~525 GHz with a *Q* of ~5 (THz system). The THz imaging system is similar to that which we have reported previously

[3] and has produced spatially resolved, relative measurements of TWC in rat burn models [1], [8]–[12]. The millimeter wave system has previously been used to explore the validity of effective media theory [13] and the utility of 100 GHz CTWC sensing *in vivo* [4]. Due to the size of the focused spot, the THz system was used to acquire images of a ~20 mm diameter area of the cornea while the 100 GHz system was utilized as a point measurement device confined to the corneal center.

A. Millimeter Wave (100 GHz) Reflectometer (Q~50)

The details of this system have been reported previously [4] and are summarized below. A block diagram of the millimeter wave reflectometer is shown in Fig. 1(a). The source was a WR 10 waveguide-mounted Gunn diode from Spacek labs[1] which transmitted a linearly polarized beam through a pyramidal feedhorn having a FWHM of ~10 deg and an average output power of ~10 mW. The 100 GHz radiation was collimated and focused onto the target at a 20 deg incidence angle using a pair of 50 mm diameter, 100 mm focal length plano-convex teflon (PTFE) lenses. Reflected illumination was collected by a second pair of plano-convex PTFE lenses and focused onto a pyroelectric detector having an optical NEP of ~1 nW [2] [Fig. 1(b)].

The Gunn diode was frequency modulated with a 1 kHz triangle wave with engineering amplitude modulation to produce a flat RF bandwidth of ~3 GHz (Fig. 1(c)). Although the video bandwidth of the pyroelectric detector was 10 Hz, the device displayed significant 1/f noise up to ~25 Hz. As a result, a low frequency amplitude modulation at 30 Hz was also employed. The output of the pyroelectric detector was fed into a lock-in amplifier with a 1 ms time constant resulting in an effective data acquisition rate of ~10 Hz (limited by lock-in settling time and amplitude modulation period) and an effective noise equivalent power of ~ 100 $nW/Hz^{1/2}$.

This arrangement produced ~66 sweeps through the RF spectrum in one on-cycle of the amplitude modulation, effectively providing a time averaged broadband signal to the detector and mitigating detrimental coherence effects that arise from the narrow instantaneous source line width and the non-zero Q and broad band optics train. The post detection signal to noise ratio (SNR) was ~30 dB. Knife edge measurements confirmed a 10%–90% spot size of ~4.5 mm, a diameter slightly smaller than the 5 mm diameter of the ultrasound pachymetry probe.

B. Reflective THz Imaging System (Q~5)

A block diagram for the THz imaging system and its corresponding illumination geometry is displayed in Fig. 2(a) and Fig. 2(b), respectively. The THz source, receiver electronics, and system design have been reported previously [3] and are summarized below.

The photoconductive switch was pumped by ~8 mW average power from a 780-nm pulse train created by a frequency-doubled 1550-nm mode-locked laser with a ~230 fs pulse width and 20 MHz repetition frequency. The chip was mounted on the backside of a silicon hyper-

---

[1]http://spaceklabs.com/cm/Products/Frequency_Sources/Gunn%20Oscillators.html.
[2]https://www.gentec-eo.com/products/thz-detectors

hemisphere and the free space output was collimated by a 76.2 mm effective focal length (EFL) off-axis parabolic (OAP) mirror. The beam is focused onto the target using a 50.8 mm EFL OAP mirror at a ~14 degree incidence angle (Fig. 2(a) The reflected radiation was collimated by a second 50.8 mm EFL OAP and then focused with a 25.4 mm EFL OAP to the feedhorn of a WR1.5 waveguide mounted Schottky diode detector. The rectified THz pulses were amplified with 38 dB of gain and coupled to a gated receiver driven with a reference RF pulse generated using a beam sampler, 1550-nm high-speed photodiode, and RF pulse amplifier.

This system architecture yields an effective THz operational band proportional to the photoconductive switch power spectral density weighted by the Schottky diode spectral responsivity (Fig. 2(c) [3]). Pixels were acquired with a 1 ms integration time and imagery was generated by raster scanning the animal model beneath the fixed, focused THz beam using x and y axis stepper motors. A diffraction limited spot size of 1 mm at a 36 mm standoff distance was measured with a knife edge target. A peak SNR of >40 dB was measured using a 1 ms integration time.

C. System Sensitivity Analysis

We have published previously on the sensitivity of both the millimeter-wave [14] and THz imaging systems [3] to changes in water content in a number of different calibration targets [15]. While these targets can be a good representation of thick, heterogeneous tissue such as skin, muscle, fat, etc., they are not optimal for cornea since it is difficult to create tissue water gradients and striated structures that accurately mimic the *in vivo* cornea. However, drying targets provide a straightforward, application-relevant method of measuring the millimeter wave and THz imaging systems sensitivities to changes in reflectivity by producing very small drops in the reflectivity in an observable manner.

In previous publications we were interested in the system Noise Equivalent Delta Water Content (NE WC) where the assumption was that the tissue of interest mimics a half space (no index discontinuities in the thickness dimension) and that changes in tissue water content are distributed evenly throughout the probing depth of the millimeter wave or THz imaging system. Due to the non-monotonic behavior of corneal reflectivity as a function of thickness and CTWC arising from etalon effects, and the desire to resolve the etalon in measurements, it is more appropriate to look at the Noise Equivalent Reflectance Difference (NERD) which imposes a systematic limit on how small a change in reflectance can be resolved.

In these experiments a 0.15 mm thick polypropylene towel was saturated with water and the reflectivity and weight of the target were measured until the target weight had dropped to its dry value. The polypropylene (PP) towel was chosen because of its tiny fibers and frequency independent index [16] provide a low-loss, nearly dispersion-free target constituent across the frequency bands of interest. The thinness of the towel was desired as it limited the development of a water content gradient during the drying process, which was undesirable for characterization as it complicates the modeling. The THz setup flattened the towel against a 13 mm thick, solid PP slab while the millimeter-wave setup suspended the towel across open air. The THz system utilized OAP mirrors and a detector with a wavelength-

sized aperture, and thus is sensitive to changes in target height. To compensate this effect, the rigid, low reflectivity (index) PP slab was selected to ensure flatness and reduce the influence from standing waves at high water fill factors (this setup demonstrates significant etalon effects at lower water fill factors [17]).

The millimeter wave system employed dielectric lenses and a large aperture (>5 mm) pyroelectric detector and thus was significantly less sensitive to target height. Additionally, the shorter optical path length (within the towel) and reduced loss presented by the wetted towel, as compared to the THz system, lends increased sensitivity to the presence of a backing. Thus a suspended target mounting was desired. The difference in mount backing provides the added benefit that the measured reflectivity ranges overlap. This facilitates analysis of system performance on similar parts of the Fresnel coefficient curves due to transmission losses.

The results of the drying experiments over a range of water content fractions relevant to the cornea are displayed in Fig. 3. Two features are immediately apparent. First the slopes of each system are significantly different with the millimeter wave system displaying ~0.78%/% and the THz system displaying ~0.15%/%. This is associated with the large difference in water dielectric function between the two bands.. Second, the measurement noise variance of the THz system is ~2.5× larger than that of the millimeter wave system. While receiver architectures, power levels, components, NEPs, etc. are starkly different between the two systems, the superior performance of the millimeter wave system is attributed to differences in post detection bandwidth, which is orders of magnitude lower (30 Hz versus ~10 GHz) than the THz system due the benefits of lock-in detection.

In this work, we choose to ascertain system NERD through regression analysis as described in (1) [14] where y_i are the reflectivity measurements, at a particular water content, f_i is the least squares fitted line evaluated at the same water content, SSE is the sum of square errors between the measurement and fit, and N is the total number or points used to compute the fit [14].

$$\text{NERD} = \sqrt{\frac{SSE}{N}} = \sqrt{\frac{1}{N}\sum_{i=1}^{N}[y_i - f_i]^2} \quad (1)$$

$$\text{NE}\Delta WC = \text{NERD}\left(\frac{dR_s}{dp_w}\right)^{-1}. \quad (2)$$

Equation (2) describes the system NE WC for a particular NERD where R_s is the measured sample reflectivity and p_w is the water content [14]. While the NE WC derived from the NERD for the towel target is not directly applicable to the cornea due to the diffusion air in the towel target and differences between the material stack and the layered structure of tissues pertinent to CTWC it is instructive to demonstrate inherent differences associated with the choice of center frequency.

The sensitivity characterization results are displayed in Table I. The millimeter wave system displays a NERD of 0.0587% and the THz system a NERD of 0.1204%.

III. Dielectric Window

All THz imaging results of animal models reported in the literature were obtained with a dielectric window pressed firmly against the tissue of interest to flatten the object plane. Prior to implementing a window, the feasibility of imaging cornea without flattening was explored through reflective imaging of a curved cornea phantom target (Fig. 4). The phantom target consisted of an 18 mm diameter PTFE sphere with highest point of the sphere positioned in the focal plane of the imaging system. This diameter was chosen because the corresponding radius-of-curvature matches that of the average human cornea. Note that there is no water in this phantom model as this experiment was intended to isolate the effect of geometry.

A THz image of the cornea phantom is displayed in the left panel of Fig. 4 where red corresponds to the highest reflectivity and blue the lowest. The highest reflectivity pixel corresponds to coincidence of the transmitter focused spot and receiver (back-projected) spot on the surface of the sphere. Inspection of Fig. 4 illustrates the rapid drop of received signal away from the coincidence condition. Within a few pixels the intensity falls far below the maximum. This effect is especially problematic in the context of imaging for corneal diseases, which requires a water content sensitivity of 1% and below [5], corresponding to a noise equivalent reflectivity difference (NERD) of ~0.1%. Reflectivity variations due to water concentration are nearly impossible to discern while signal variation is dominated by geometric variation. This precipitous signal drop can be attributed to the off axis parabolic mirrors used in THz imaging systems. These elements are well known to behave poorly when the target surface normal is not correctly aligned with the focal axis. Preliminary ray tracing and physical optics work suggest that the significant drop in signal is due to the reflected energy not making it to the detector plane.

To quantify this effect, horizontal and vertical cuts were sampled from the paths denoted by the white dotted lines on the left side of Fig. 4, and are displayed on the right side. Superimposed on each cut are Gaussian fits. The standard deviation (~0.896 mm), the same for both cuts, was corrected for the increased width due to the blurring kernel used for image de-noising (Gaussian with $\sigma = 0.24$ mm). This yielded a 1/e fullwidth of $2\sigma = 1.73$ mm, a FWHM of 2.03 mm and 10–90 full width of ~1.42 mm. Note that the 10%–90% spot size of the system is 1.1 mm.

From these imaging results it is evident that the poor performance of THz imaging systems when imaging significantly curved surfaces necessitates the use of a window to flatten the field. While contact is inconvenient for clinical application, its use is not unprecedented and there are many examples of ophthalmologic imaging systems, such as confocal microscopy, that employ the use of rigid corneal flattening windows [18], [19].

One final point regarding the dielectric window is it's interaction with the tear film. The low contact pressure provided by the window combined with the speculum used to keep the eye open was assumed to eliminate the tear film since the natural blink reflex could not replenish

the film. However, the window also acts as a barrier and constrains moisture loss from the epithelium. Our experimental setup is thus well suited to a first pass imaging trial of the cornea as measurement of corneal tear film thickness is challenging and a clinically accepted technique has not yet been adopted.

IV. *In Vivo* Trials

In vivo studies were approved by the local Institutional Animal Care and Use Committee (IACUC) and were performed with white New Zealand male rabbits which are a common model for the human cornea [20]–[22] and because of similarities in size, shape, and CTWC. Five rabbits were anesthetized using 30 mg/kg and 5 mg/kg of Ketamine and Xylazine, respectively, followed by intubation with a 1.5 mg/ml flow of Isofluorane. Each rabbit was placed in turn on an imaging cart with the head support panel adjusted to accommodate the rabbit's neck and head, and secure the intubation tubes (Fig. 5).

Next, the right eye was held open and dehydration was invoked using a gentle air blower for 15 min. A Mylar window 12.7-μm thick was then lowered onto the cornea's surface to secure it in place and conform it to a horizontal planar geometry with respect to the imaging optics. The following measurements were then obtained in the listed order every 10–20 min for the subsequent imaging period.

1. *Thickness measurement:* Average of 5 readings using the ultrasound pachymeter. These measurements (± 5 μm accuracy) were through the Mylar window and the substrate thickness was subtracted out.

2. *Millimeter-wave point reflectivity:* Average of 100 mmm-wave reflectivity measurements obtained with the aforementioned 100-GHz reflectometer. A class I, 650 nm targeting laser was employed to ensure co-alignment of transmit and receive 100-GHz beams.

3. *THz reflectivity maps:* A THz image of a 20 mm×20 mm object area was obtained with 0.5-mm-wide pixels. This area was intentionally made larger than the cornea/window contact for the monitoring of system drift and noise through analysis of pixels along the periphery.

The thickness and 100 GHz point measurements each required ~1 minute acquisition time while the THz imaging required ~5 min. With the Mylar window separating the epithelium from the outside environment, the dehydrated cornea was assumed to increase in TWC to a slightly hyper-hydrated state over the course of one to two hours.

A. CCT Calculations

While rabbit corneas are a very good physiologic model of human cornea in terms of their healthy TWC and radius of curvature, they are, on average, thinner than healthy human cornea, ranging from ~0.3 mm to ~0.5 mm as compared to the ~0.45 mm to ~0.7 mm for human cornea. A modified CCT to $\overline{\text{CTWC}}$ equation taking this difference in thickness is given in (3) with the same functional form as the clinically employed human (4).

$$\begin{aligned}
\overline{\mathrm{CTWC}}_{\mathrm{rabbit}} &= \frac{CCT - 0.075}{CCT + 0.062} \\
CT &\sim \varepsilon[0.3, 0.5]
\end{aligned} \quad (3)$$

$$\begin{aligned}
\overline{\mathrm{CTWC}}_{\mathrm{human}} &= \frac{CCT - 0.091}{CCT + 0.051} \\
CT &\sim \varepsilon[0.45, 0.7].
\end{aligned} \quad (4)$$

Little data exists regarding the theoretical and/or practical limitations of these equations. The ones denoted here are based on a rough survey of the literature and should not be interpreted as exact limits. A plot of both (3) and (4) are displayed in Fig. 6 with linear fits, calculated over the appropriate thickness ranges, superimposed on the curves as non-overlapping shaded regions.

Equation (3) was used throughout the experiment to estimate CTWC from ultrasound CCT measurements.

B. CCT Measurements

The CCT measurements for all five rabbits are displayed in Fig. 7. The data points represent averages of 5 measurements for each time point, which was done to overcome variance intrinsic to contact probe measurements. Linear fits are superimposed on the data points. Each rabbit displayed an increase in CCT as a function of time with an average rate of ~25.6±4 microns per hour indicating protocol consistency.

The corresponding mean TWC of the cornea ($\overline{\mathrm{CTWC}}$) is displayed on the right axis of Fig. 7 as computed with (3). Note that the mapping from CCT to $\overline{\mathrm{CTWC}}$ is nonlinear resulting in a compressed TWC vertical scale. One important point apparent from Fig. 7 is the variance in CCT of the five different rabbit cornea at the start of the experiment reflecting the large physiologic variation of *in vivo* corneas. The thickness in the healthy corneas range from 0.373 to 0.425 mm ($N = 5$ measurements per quoted healthy thickness value), for which (3) predicts a CTWC range from 76.8% to 79.4%. This was assumed to be entirely due to natural physiologic variation of healthy cornea as all animals were determined by the attending veterinarian to have healthy corneas just prior to anesthesia and the commencement of experiments. A $\overline{\mathrm{CTWC}}$ value of 76.8% suggests compromised corneal health whose deteriorated state would be detected upon visual inspection. This further illustrates the inaccuracy of the thickness-to-CTWC mapping on which all pachymetry is based.

C. 100 GHz Results

The results of the millimeter wave point measurements are displayed in Fig. 8 where the reflectivity has been plotted against pachymetric CCT measurements indicated on the bottom *x*-axis, and estimated $\overline{\mathrm{CTWC}}$ indicted on the top *x*-axis. Strong, positive correlation between increasing CCT and increasing millimeter wave reflectivity was observed. Linear fits were superimposed on the data corresponding to the hypothesized approximate linear increase in millimeter wave reflectivity with linear increase in $\overline{\mathrm{CTWC}}$ [4].

Although the increases in Fig. 7 and Fig. 8 display good correlation, the ensemble of millimeter wave reflectivity slope magnitudes appear to have more fractional variation than the ensemble of CCT slope magnitudes. In other words, the mm-wave signal is changing between rabbits much more than the CCT measurements. If this signal variation is due to real physiologic variation, the millimeter wave measurement may have significantly greater sensitivity and/or larger dynamic range than corneal pachymetry. Conversely, as mentioned previously, the mapping from CCT to $\overline{CTWC}$ is inherently inaccurate, which may be due entirely to the limitations of (3).

D. Reflective THz Imaging

Six THz images from each of the five rabbit models acquired throughout the experiments are shown in Fig. 9 with a standard false color pallet (color online) where red areas correspond to increased reflectivity and blue areas to decreased reflectivity. Each set has been normalized to its individual global maximum. The CCT measurement range and corresponding estimated CTWC range computed with (3) has been noted next to each image set. The top left image in each series was acquired at time 0 and the last image in each series is located in the bottom right where time is incremented from left to right, top to bottom with the total elapsed time from image 1 to image 6 ranging from 100 to 160 min.

The images reveal noticeable, spatially varying shifts in reflectivity contrast throughout the cornea for the duration of the experiment. The perimeter of the cornea also changes with time suggesting that the corneal thickness is sufficiently perturbed to increase the total surface area touching the window as swelling occurs. As mentioned above, the corneal flattening window was applied with light contact pressure to minimize the effect of the window on corneal physiology. We hypothesize the following for the spatial gradient in contrast.

1. The variation in reflected signal as observed radially from the center of the cornea outwards is likely due to variations in corneal thickness as the cornea is known to increase in thickness from the center to the periphery [7].

2. The gradient observed from one side of the cornea to the opposing side may also be due to variations in corneal thickness. Additionally, the gradient may arise from the window coupled cornea not being perpendicular to the THz radiation leading to a variation in illumination angle across the imaging field. Finally, it is possible that the center of the cornea did not lie coincident with the imaging plane.

Bubble levels were employed to maximize the co-linearity of the window normal with the imaging system optical axis and visual inspection was relied on to monitor any curvature in the window coupled cornea arising from the thinness of the mylar window (minimal "bulging was observed"). Additionally, the attending veterinarian was consulted for each window placement to minimize the deviation between the location of the corneal apex and the center of the FOV. Due to the difficulties of *in vivo* experiments. These factors cannot be ruled out but they were minimized to the best of our ability.

All of these factors can be minimized with the integration of an optical coherence tomography based (OCT) imaging pachymetry system which can provide a complete

thickness map across the full extent of the cornea although image registration between modalities remains a challenge. Efforts are currently underway to add this measurement capability to the experimental protocol.

E. Region of Interest Analysis

A region of interest (ROI) is indicated by the dashed circle in the first image of each series in Fig. 9. The diameter matches that of the ultrasound beam created by the pachymetry probe, and the location indicates the interrogated area. In addition to laser targeting, small fiducial markers (transparent to THz illumination) on the Mylar window helped ensure repeatable probing location. The imaged area was intentionally larger than the rabbits' corneas, guaranteeing the absence of cornea in the periphery of the images and allowing for accurate monitoring of system drift and noise.

To confirm accurate placement of the ultrasound probe, image processing techniques were utilized to verify its location at the apex of the cornea. The THz cornea images were converted to binary masks using a threshold four times larger than the standard deviation of the pixels located in the corners of each image area. The resulting masks were morphologically closed using a disc-shaped structuring element. Then, the centroids of the cornea masks were computed, and a circular mask with a radius corresponding to the pachymeter's radius (5 mm) was placed at the centroid, creating the pachymeter test mask. This result was compared to registered visible images of the fiducials markers against the cornea under test. The mean reflectivities and standard deviations in the pachymeter mask and in the cornea mask were then computed and confirmed to be statistically insignificant.

The average reflectivity signal of these ROIs are displayed in Fig. 10 where the larger error bars correspond to the variation within the pachymeter mask, and the smaller error bars are the variation due to system noise assuming it is dominated by the thermal noise of the Schottky-rectifier front-end [23]. A zoom-in of one of the data points on the left-hand side of Fig. 10 demonstrates the difference in magnitude between the variation within the cornea mask and the system noise.

A number of interesting features are observed in these companion plots. First, the error bars computed from data points within the region of interest are significantly larger than those plotted for the millimeter wave measurement in Fig. 8. However, the signal-to-noise ratio (SNR) of each system is comparable as evidenced by the similar noise error bars. This result indicates that the majority of the variance in signal amplitude within the ROI arises from the spatial variation of the corneal reflectivity (i.e. real signal); even if the ultrasound probe could be scanned the contact area is too large to capture the spatial variation of cornea properties.

However, the most surprising result of the ROI plots is the nearly zero correlation between THz reflectivity and CCT measurements. Rabbits 1 and 2 display slight increases in reflectivity while rabbits 3, 4, and 5 display slight decreases. In both cases the total change is, at maximum, nearly an order of magnitude less than the variance.

F. Sensitivity Calculations

As a comparison of system performance, the thickness sensitivity of each system was computed using the slope of the regression line fit to each rabbit data set and the variance about each point. The $\mathrm{CCT}/\overline{\mathrm{CTWC}}$ relationship described in (3) and (4) is approximate so it is more appropriate to compute sensitivity in terms of CCT directly. As discussed in our companion publication [6], any path through the entire $\mathrm{thickness}/\overline{\mathrm{CTWC}}$ space generally produces a nonlinear profile. However, linear functions provide a high goodness of fit over the limited thickness range variation observed.

$$\mathrm{CCT}_{sens.} = \frac{\max(\sigma_n)}{\frac{df_n}{dCCT}}. \quad (5)$$

Thickness sensitivity was computed using (5) where is $\max(\sigma_n)$ the maximum standard deviation observed in rabbit n and $df_n/dCCT$ is the slope of the regression line for rabbit n. The results are tabulated below.

These results suggest that millimeter-wave-reflectometry-based CTWC measurements are anywhere from one to two orders of magnitude more sensitive than those acquired with the 525 GHz system. Furthermore, the sensitivity of the THz imaging system was calculated to be negative in two out of the five rabbits. This statistically insignificant change in THz signal paired with a significant increase in millimeter wave signal with thickness suggests that signal variation cannot be attributed entirely to shifts in $\overline{\mathrm{CTWC}}$.

V. Analysis

To explore the source of variation in the data, the $\overline{\mathrm{CTWC}}$-thickness reflectivity spaces presented in [6] were recomputed for the operating spectra of both systems with the 12.7 μm thick Mylar window included in the stratified media model. The spaces are displayed in Fig. 11 with corresponding constant thickness, constant $\overline{\mathrm{CTWC}}$, and CCT paths plotted using (3).

The millimeter wave spaces are very similar to those presented in [6] owing to a time averaged RF bandwidth that is roughly rectangular but still symmetric. The THz spaces are similar to the Q = 5 system in [6] albeit with slightly larger maximum reflectivities and reflectivity ranges. This difference arises from the photoconductive switch PSD and Schottky diode spectral responsivity which are heavily skewed towards the lower frequencies, thus accessing larger overall tissue reflectivities and TWC sensitivities.

A. Thickness Variations

The ultrasound pachymeter used in these experiments relies on a pulse echo methodology with range gating [24] to ascertain the axial location of the acoustic impedance discontinuity at the endothelium/aqueous humor interface. None of the steps in the protocol were thought to have compromised this discontinuity, so thickness values extracted by our ultrasound measurements were assumed to be accurate. Therefore, only the constant $\overline{\mathrm{CTWC}}$ paths and CCT projections were analyzed.

The expected reflectivity of cornea as a function of thickness, averaged over the operational band of both the millimeter wave and THz imaging systems are displayed on the left-hand and right-hand sides, respectively, of Fig. 12 using a volumetric average CTWC of 79.4%. Comprehensive analysis requires one to analyze a family of curves at varying constant CTWC percentages. However, since experimental calibration to determine accurate absolute reflectivity is difficult, it is instructive to instead look at the trends of changes in relative CTWC. In this case, constant $\overline{\text{CTWC}}$ profiles at 77%, 78%, 79%, 80%, 81%, etc., produce nearly identical variation trends within a particular band. Thus fixing the analysis to 79.4% is sufficient.

Over the range of thicknesses measured experimentally (0.375 mm to 0.475 mm), if the $\overline{\text{CTWC}}$ remains constant, the millimeter wave system is predicted to measure an increase in reflectivity as corneal thickness increases. Similarly, if $\overline{\text{CTWC}}$ and thickness are increasing simultaneously all three candidate distributions yield monotonically increasing reflectivity.

In contrast, the THz system is predicted to measure a minor decrease in reflectivity as the corneal thickness increases from 375 to 400 μm, followed by a minor increase in reflectivity as corneal thickness increases from 400 to 475 μm. However, the total variation is <0.05% which is beyond the measured NERD (Section II-C) of the THz imaging system. When simultaneous $\overline{\text{CTWC}}/\text{thickness}$ increases are considered the pinned front gradient type displays similar behavior with a total variation of <0.1% while the pinned back and global variation gradient types display significant increases over the range with a predicted gain of >0.5%; a factor of four larger than the measured NERD.

The protocol employed external means to perturb CTWC; namely blowing dry air and application of a dielectric window. Further, histologic analysis of the tissue post experiment confirmed that none of the protocol steps affected the deeper layers of the cornea. Thus we can conclude, with high confidence, that the outer layers of the cornea were most affected and that the pinned back gradient case is the most appropriate model of experimental parameters.

The millimeter-wave data matches the pinned back case quite well with statistically significant, positive correlations between CCT and reflectivity. The THz system displayed a slight increase in reflectivity from ~0.375–0.400 mm, followed by a slight decrease in reflectivity from ~0.400–0.475 mm which is inverted from what is predicted by Fig. 12. However, the variance of the results indicate statistically insignificant changes for all rabbit models which is predicted by the Fig. 12 considering constant CTWC.

From this ensemble of curves it is evident that the only explanation that fits the experimental observations is that the protocol was not perturbing the CTWC but appreciably modulating the thickness. While the difficulties associated with perturbing healthy CTWC without injuring corneal tissue are known [25], it is surprising that the CCT changed so significantly for an apparent lack in CTWC change. This result leads to a number of interesting observations.

To our knowledge this is the first result ever published that quantitatively investigates the potentially poor correlation between corneal thickness and CTWC *in vivo*. The lack of a one-to- one mapping between corneal thickness and CTWC and the inability of pachymetry to correct for physiologic variation is well known, yet this represents the first *in vivo* study with quantitative observations of the inaccuracies.

Second, while the center areas of each cornea display minimal changes in reflectivity (CTWC) the perimeters of some of the samples show marked changes throughout the duration of the experiment. Standard corneal physiology tells us that the perimeter of the cornea is anywhere from 9% to 52% thinner than the central corneal dimension. It is possible that the reflectivity changes at the edges of the cornea and/or decreases as predicted by our modeling efforts correspond to thickness variations. Replacing ultrasonic pachymeter spot measurements with OCT based pachymetry which can provide full 3D characterization the entire corneal geometry will help improve the accuracy of the measurements by allowing the resolution of spatially varying etalons.

Third, as discussed previously, the refractive index of the non-water constituents of cornea at THz frequencies are not well characterized. Similarly, the ratios of bound to unbound water *in vivo* is also not known. Shifts in refractive index will change the free spectral range (FSR) of the lossy cornea cavity, thus shifting the range over which increases and decreases in THz corneal reflectivity occur in the fixed CTWC, varying thickness case.

Finally, it is likely that part of the perturbation observed in corneal thickness was caused by the use of the Mylar window which applies a very slight pressure to the cornea although care was taken to ensure the window applied the same pressure as a corneal probe. This observation indicates that THz or millimeter wave CTWC studies may require non-contact, windowless system architecture. This requirement presents a significant engineering design challenge to systems/optical engineers given the poor performance of traditional THz medical imaging system design when interrogating curved surfaces.

VI. Next Steps: Preliminary Post Mortem Study

Sections III and IV identified the hypothesized dominant role of varying optical path length and the minimal role of CTWC in the reflectivity signals observed in healthy cornea experiments. To further elucidate the role of corneal tissue geometry on reflectivity signal we performed a preliminary experiment on one additional rabbit using the millimeter wave reflectometer.

The animal model was prepared with the same protocol discussed in Section III. Following gas anesthesia an ensemble of healthy CCT measurements were acquired and yielded a mean of 0.42 mm. The animal was then euthanized. Once death was confirmed five pairs of CCT and millimeter wave reflectivity measurements were obtained over the course of 45 minutes.

The goal of the five animal experiments was to assess the performance of THz and millimeter wave reflectometers when presented with live healthy cornea. The aim of this experiment was to initiate a change in corneal thickness that was paired with a definite

change in CTWC and whose change in CTWC resulted in the occurrence of an observable etalon. When the rabbit dies, the cornea begins to lose water through the top side of the cornea due to disappearance of the tear film while also experiencing a gain in CTWC from the backside due the death of the endothelium and subsequent diffusion. In this experimental setup, the presence of the Mylar window prevents water from evaporating from the front side, ensuring that the CTWC changes only on the backside the cornea swells as CTWC increases [6]. This protocol recreates the pinned front CTWC gradient type introduced in [6] and discussed in Section IV of this publication. Note that the CCT projection for the pinned front gradient type (Fig. 12) predicts a maximum reflectivity at ~0.483 mm assuming a baseline $\overline{\text{CTWC}}$ of 79.4%.

The millimeter wave system was chosen because our NERD characterization suggested sufficient sensitivity to detect the expected variation in reflectivity and one system was desired to minimize the effects of movement when switching between imaging modalities.

The results of the experiment are displayed in the left side of Fig. 13 and predicted pinned front behavior is plotted in the left side of Fig. 13 with a swing in reflectivity that is ~ a factor of 5 larger than our noise limited reflectivity difference (NERD). A significant increase in reflectivity was observed followed by a significant decreases as the CCT ranged from 0.441 to 0.475 mm. The data suggests that a maximum in reflectivity occurred somewhere between 0.457 and 0.469 mm which is 0.014 to 0.026 mm offset from the predicted maximum.

The offset in peak position could be due to a number of factors including an oversimplification or error in assumption of the pinned front gradient profile, error in CCT measurement, flaws in the application of effective medium theory or, likely, deviations between the CCT-CTWC predicted by (3) and the correct *in vivo* relationship. Additionally, a small differential between the assumed and actual refractive index of the non-water tissue constituents (primarily collagen) can swing the predicted peak closer to or further to from the observed peak.

One animal does not allow conclusions to be drawn on deviations between tissue models and *in vivo* results. However, a large ensemble of CTWC gradient and CTWC/CCT pairs predict a thickness based standing wave when plugged into the effective media theory model and the observed results are compelling.

The exploration of coupled relationship existing between CCT and CTWC are pertinent to the next stage of this work due to the clinically measured increase CCT and assumed increase in $\overline{\text{CTWC}}$ inferred from observed visible light scattering. Invasive measures are the only known method of inducing these coupled changes and work is underway to quantify the sensitivity of millimeter wave and THz imaging to these changes.

VII. Conclusion

A study of the utility of THz imaging and millimeter wave reflectometry for the measurement of CTWC was performed with five rabbit models. To our knowledge these are the first THz images ever published of cornea *in vivo*. A protocol was implemented to

dehydrate and then hyperhydrate healthy cornea over the course of 1–3 hours during which clinically accepted ultrasound pachymetry measurements mapped thickness to CTWC. Companion millimeter wave reflectivity spot measurements and THz reflectivity maps were also obtained. Increases in millimeter wave reflectivity and thickness were noted with good correlation. THz $\overline{CTWC}$ maps, however, displayed marked reflectivity increases in some areas, decreases in others, and a relative lack of CTWC change in the region probed with the pachymeter. Electromagnetic modeling suggests that the protocol changed the thickness of the cornea but not the CTWC. These results are the first experimental indication that trends in corneal thickness do not necessarily correlate with changes in CTWC gradients or $\overline{CTWC}$.

CTWC sensing and imaging represents a key opportunity to the field of THz medical imaging because of the low physiologic variation in tissue constituents (compared to skin, lung, liver, etc.) and the non-trivial physiologic variation in thickness that renders clinically accepted techniques such as pachymetry inaccurate. However, the location of the aqueous humor immediately below the cornea can present a stratified media target or a half space depending on operational parameters such as frequency, angle of incidence, CTWC etc. which can markedly change the computed CTWC due to the structural similarity with optical thin films. For this reason, we hypothesize that the most accurate CTWC sensing system architectures will follow one of two possible types.

1. Reflectivity maps at multiple frequencies are acquired and correlated with spatially resolved thickness maps obtained with OCT.

2. Reflectivity maps at multiple frequencies are acquired and modeling is used to obtain both CTWC and thickness maps simultaneously.

A single frequency or single band integrated measurement is not sufficient for decoupling CTWC based signal variation from CCT based signal variation. Further, contact between the imaging/sensing system and cornea confounds the aggregate RF properties. Non-contact, spectrally resolved measurements are imperative for resolving contribution from different mechanisms and engineering work is underway to integrate frequency swept transceivers with novel scanning architectures.

Acknowledgments

References

1. Tewari P, Kealey CP, Bennett DB, Bajwa N, Barnett KS, Singh RS, et al. In vivo terahertz imaging of rat skin burns. J Biomed Opt. 2012; 17:040503–3. [PubMed: 22559669]

2. Taylor ZD, et al. Reflective terahertz imaging of porcine skin burns. Opt Lett. 2008; 33:1258–1260. [PubMed: 18516193]

3. Taylor ZD, et al. THz medical imaging: In vivo hydration sensing. IEEE Trans THz Sci Technol. Sep; 2011 1(1):201–219.

4. Bennett D, Taylor ZD, Tewari P, Sung S, Maccabi A, Singh R, et al. Assessment of corneal hydration sensing in the terahertz band: In vivo results at 100 GHz. J Biomed Opt. 2012; 17:097008–1.

5. Bennett DB, et al. Terahertz sensing in corneal tissues. J Biomed Opt. 2011; 16:Art. ID 057003.

6. Taylor ZD, et al. THz sensing of corneal tissue water content: Modeling and analysis of electromagnetic properties. TIEEE Trans THz Sci Technol. 2015; 5

7. Thomas, CI. The Cornea. Springfield, IL, USA: Thomas; 1955.

8. Bajwa, N., et al. Reflective THz and MR imaging of burn wounds: A potential clinical validation of THz contrast mechanisms. SPIE THz Emitters, Receivers, and Appl. III; San Diego, CA. 2012. p. 84960X

9. Taylor, ZD., et al. THz imaging using broadband direct detection. SPIE THz, RF, Millimeter, and Submillimeter-Wave Technol. and Appl. VI; San Francisco, CA, USA. 2013.

10. Tewari, P., et al. Medicine Meets Virtual Reality. Long Beach, CA, USA: 2011. Terahertz imaging of biologic tissues; p. 653-657.

11. Taylor, ZD., et al. THz Medical Imaging. 6th ESA Workshop on Millimetre Wave Technol. and Appl. and 4th Global Symp. on Millimeter Waves; Helsinki, Finland. 2011.

12. Tewari, P., et al. Advances in biomedical imaging using THz technology with applications to burn-wound assessment. SPIE THz Technol. Appl. V; San Francisco, CA, USA. 2012. p. 82610T-82610T.

13. Maccabi, A.; Bennett, DB.; Bajwa, N.; Tewari, P.; Sung, S.; Singh, RS., et al. Reflectivity measurements of water and dioxane mixtures using a 100 GHz gunn diode source. SPIE THz and Ultrashort Electromagn. Pulses for Biomedical Appl. I; San Francisco, CA, USA. 2013.

14. Sung, S., et al. Reflective measurement of water concentration using millimeter wave illumination. SPIE Health Monitoring of Structural and Biological Syst; 2011; San Diego, CA, USA. 2011. p. 798434

15. Taylor, ZD.; Singh, RS.; Culjat, MO.; Suen, JY.; Grundfest, WS.; Brown, ER. THz imaging based on water-concentration contrast. SPIE THz for Military and Security Appl. VI; Orlando, FL, USA. 2008. p. 69490D-8

16. Lamb JW. Miscellaneous data on materials for millimetre and submillimetre optics. Int J Infrared and Millimeter Waves. 1996; 17:1997–2034.

17. Bennett DB, Li W, Taylor ZD, Grundfest WS, Brown ER. Stratified media model for terahertz reflectometry of the skin. IEEE Sensors J. May; 2011 11(5):1253–1262.

18. Cavanagh HD, Petroll WM, Alizadeh H, He YG, McCulley JP, Jester JV. Clinical and diagnostic use of *in vivo* confocal microscopy in patients with corneal disease. Ophthalmology. 1993; 100:1444–1454. [PubMed: 8414403]

19. Malik RA, et al. Corneal confocal microscopy: A non-invasive surrogate of nerve fibre damage and repair in diabetic patients. Diabetologia. 2003; 46:683–688. [PubMed: 12739016]

20. Xiong C, et al. A rabbit dry eye model induced by topical medication of a preservative Benzalkonium Chloride. Investigative Ophthalmol & Visual Sci. May 1.2008 49:1850–1856.

21. Hunter PA, Garner A, Wilhelmus KR, Rice NS, Jones BR. Corneal graft rejection: A new rabbit model and cyclosporin-A. Brit J Ophthalmol. May 1.1982 66:292–302. [PubMed: 7041957]

22. Gimbrone MA, Cotran RS, Leapman SB, Folkman J. Tumor growth and neovascularization: An experimental model using the rabbit cornea. J National Cancer Inst. Feb 1.1974 52:413–427.

23. Hesler, JL.; Crowe, TW. NEP and responsivity of THz zero-bias Schottky diode detectors. 2007 Infrared and Millimeter Waves, and 2007 15th Int. Conf. on THz Electron. IRMMW-THz Joint 32nd Int. Conf. on; p. 844-845.

24. Ehlers N, Hjortdal J. Corneal thickness: Measurement and implications. Experimental Eye Res. 2004; 78:543–548.

25. Ruberti JW, Klyce SD. NaCl osmotic perturbation can modulate hydration control in rabbit cornea. Experimental Eye Res. Mar.2003 76:349–359.

Biographies

Zachary D. Taylor (S'06–M'09) received the B.S. degree in electrical engineering from the University of California (UCLA), Los Angeles, CA, USA, in 2004, and the M.S. and Ph.D. degrees in electrical engineering from the University of California (UCSB), Santa Barbara, CA, USA, in 2006 and 2009, respectively.

He is an adjunct assistant professor with the University of California (UCLA), Los Angeles, CA, USA, with appointments in the Department of Bioengineering, Department of Surgery, and Department of Head and Neck Surgery. He is currently conducting biomedical THz imaging research in collaboration with the departments of Neurosurgery, Neuropathology, Pathology, General surgery, and Ophthalmology at the UCLA David Geffen School of Medicine. Additionally, he is working on THz system design, THz optics design, and image processing techniques to improve THz image acquisition rates.

James Garritano received the B.S. degrees in electrical engineering and biochemistry from the University of California (UCLA), Los Angeles, CA, USA, in 2012, and is currently a graduate student Medical Imaging Informatics track in the Department of Bioengineering at UCLA and a researcher in the Center for Advanced Surgical and Interventional Technology. His research interests are THz medical imaging, image-guided therapy, image analysis, image registration, sensor fusion, and fluorescence-lifetime imaging.

Shijun Sung received the B.S. degrees in electrical engineering University of California (UCLA), Los Angeles, CA, USA, in 2011, and is currently a graduate student in the

Department of Electrical Engineering and performs research with a number of faculty members and researchers in the Department of Bioengineering and in the David Geffen school of medicine. His research interests included THz medical imaging, THz optical and quasi-optical design, THz system design, and corneal water content sensing.

Neha Bajwa received the B.S. degree in biomedical engineering from The Johns Hopkins University, Baltimore, MD, USA, with a concentration in cell tissue engineering, in 2008, and the M.S. degree in biomedical engineering from the University of California (UCLA), Los Angeles, CA, USA, in 2010, and is currently working toward the Ph.D. degree in biomedical engineering at UCLA..

She has focused her research on THz imaging for diagnostic applications in cornea and burn models. Additionally, she is investigating THz imaging for cancer margin detection and fusing THz burn data with MRI imagery.

David B. Bennett (S'11) received the B.S. degree in physics from University of California, (UCSB), Santa Barbara, CA, USA, in 2006, and the M.S. and Ph.D. degrees in electrical engineering from University of California (UCLA), Los Angeles, CA, USA, in 2008 and 2011, respectively. His thesis work produced the initial analysis of the THz properties of corneal tissue and he performed some of the first *in vivo* experiments of THz frequency corneal reflectivity.

He is currently with Fitbit, San Francisco, CA, USA.

Bryan N. Nowroozi received the Ph.D. degree in ecology and evolutionary biology from Brown University, Providence, RI, USA, in 2011.

He was a postdoctoral researcher in the UCLA Department of Bioengineering and the assistant director of graduate education at the UCLA Center for Advanced Surgical and Interventional Technology. His research interests are in medical imaging, haptic feedback, and biomechanics. He currently with Mimeo Labs Inc., Santa Monica, CA, USA.

Priyamvada Tewari received the B.S. and M.S. (Integrated Honors) degrees in biophysics from Panjab University, Haryana, India, in 2006, and the Ph.D. degree from the Department of Bioengineering, University of California (UCLA), Los Angeles, CA, USA, in 2012. The topic of her dissertation was Terahertz imaging for early detection of skin disorders and pathologies including cancer, burns, and hydration.

She is currently with Elsevier Life Science Solutions, San Francisco, CA, USA.

James W. Sayre received the Ph.D. degree in biostatistics in the department of Biostatistics, University of California (UCLA), Los Angeles, CA, USA, in 1977.

He is an Adjunct Professor of Biostatistics& Radiological Sciences at UCLA. His current research interests include computational statistics and database management, clinical trials, statistical methodology in medical diagnostic systems.

Jean-Pierre Hubschman trained in Ophthalmology at the Hopital La Timone in Marseille France from 1991 to 1996 and received theM.D. degree from Aix-Marseille University, France, in 1996.

He did a Fellowship in vitreo-retinal surgery from 1996 to 1998 and then headed the Retina department of the Ophthalmologic Center of Saint Jean de Luz—France, the Policlinique Aguilera Biarritz—France and the Policlinica Guipozcoa San Sebastian, Spain. In 2007, he joined the Retina division of the Jules Stein Eye Institute, University of California (UCLA), Los Angeles, CA, USA, as an Assistant Professor of Ophthalmology. His current research interests include development of minimally invasive surgical tools and techniques, surgical robotic systems, and ocular imaging technologies.

Dr. Hubschman is a member of the American Research Society in Ophthalmology, the European Research Society in Ophthalmology and Vision, and the American Society of Cataract and Refractive Surgery.

Sophie X. Deng received her doctor of medicine and doctor of philosophy degrees at the University of Rochester School of Medicine and Dentistry, Rochester, NY, USA, where she completed the rigorous Medical Scientist Training Program.

She did her residency in ophthalmology at the Illinois Eye and Ear Infirmary, Chicago, IL, USA. She subsequently completed her fellowship in Cornea, External Ocular Disease and Refractive Surgery at the Jules Stein Eye Institute. She is an Associate Professor in the Cornea Division at the Jules Stein Eye Institute, University of California (UCLA), Los Angeles, CA, USA. She is a specialist in corneal and external ocular diseases, and cataracts. Her surgical areas include endothelial keratoplasty (DSEK and DMEK), deep anterior lamellar keratoplasty (DALK), penetrating keratoplasty, limbal stem cell transplantation, artificial cornea and cataract. She is the director of the Conea Biology Laboratory at the Jules Stein Eye Institute. Her research focuses on corneal epithelial stem cells regulation, deficiency and regeneration. Her research aims to improve the current treatment for patients with limbal stem cell deficiency by using stem cell therapy to restore vision. In addition, she conducts clinical studies to develop new imaging and molecular tests to accurately diagnose and stage limbal stem cell deficiency.

Elliott R. Brown (M'92–SM'97–F'00) received the Ph.D. degree in applied physics from the California Institute of Technology, Pasadena, CA, USA, in 1985.

He did his post-doctoral work at Lincoln Laboratory, Massachusetts Institute of Technology. He is a Professor of Physics and Electrical Engineering at Wright State University WSU), Dayton, OH, USA, where he holds the Ohio Research Scholars Endowed Chair in Sensors Physics. He conducts research and teaching courses in RF and THz sensor science and technology, and in solid-state physics and engineering. His THz research encompasses several topics including ultra-low-noise rectifiers, photomixing sources, the THz phenomenology of biomaterials, and THz remote sensor and imager design and simulation. Other areas of research include multifunctional RF electronics and systems, biomedical ultrasonic imaging in and around hard tissue (in collaboration with the UCLA Medical and Dental Schools), and electronic and photonic transport in nanostructures. Prior to WSU, he was a Professor of Electrical and Computer Engineering at the University of California, (Santa Barbara and Los Angeles campuses), and prior to that was a Program Manager at DARPA in the Electronics Technology Office, Arlington, VA, USA.

Dr. Brown is a Fellow of the American Physical Society (since 2007). In 1998, he received an Award for Outstanding Achievement from the U.S. Office of the Secretary of Defense.

Warren S. Grundfest received the M.D. degree from the College of Physicians & Surgeons, Columbia University, New York, NY, USA, in 1980, and trained in General Surgery at University of California (UCLA), Los Angeles, CA, USA, and Cedars-Sinai Medical Center, Los Angeles, CA, USA, in 1985.

He is a Professor of Bioengineering at the University of California (UCLA), Los Angeles, CA, USA. He is also a Professor of Electrical Engineering and Professor of Surgery at UCLA. His current research interests include excimer lasers for medical applications, optical diagnostic procedures, minimally invasive surgical tools, haptic feedback and ultrasound imaging.

Dr. Grundfest was elected Fellow, American Institute of Medical & Biologic Engineers (AIMBE), for pioneering development and dissemination of minimally invasive surgery in 1996. In the same year, he was elected Fellow, Society of Photo-Optical Instrumentation Engineers (SPIE), for his distinguished & valuable contributions to the field of optical engineering in medicine & biology.
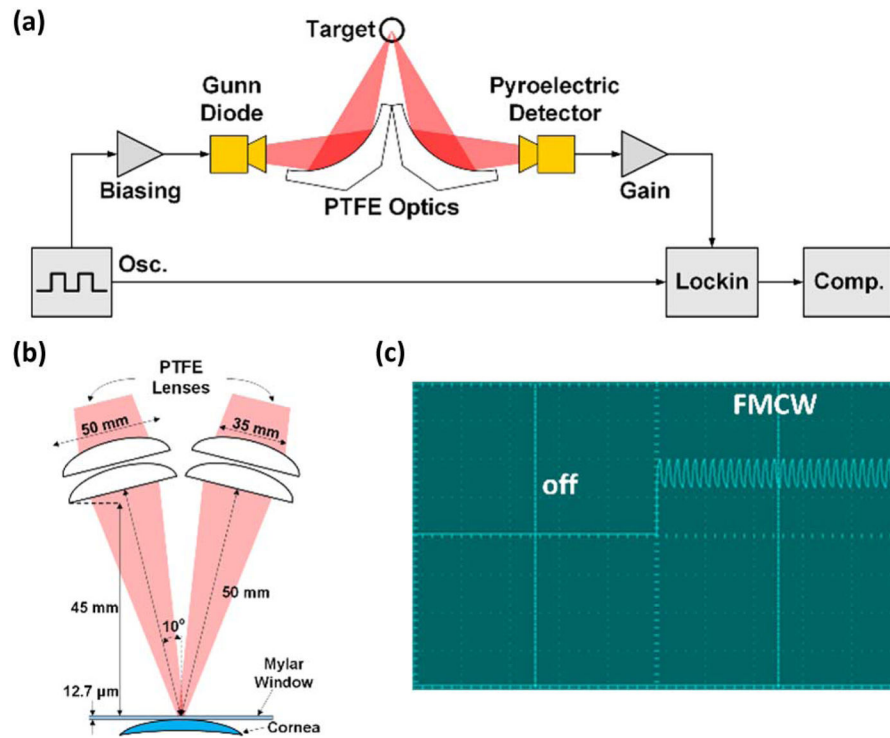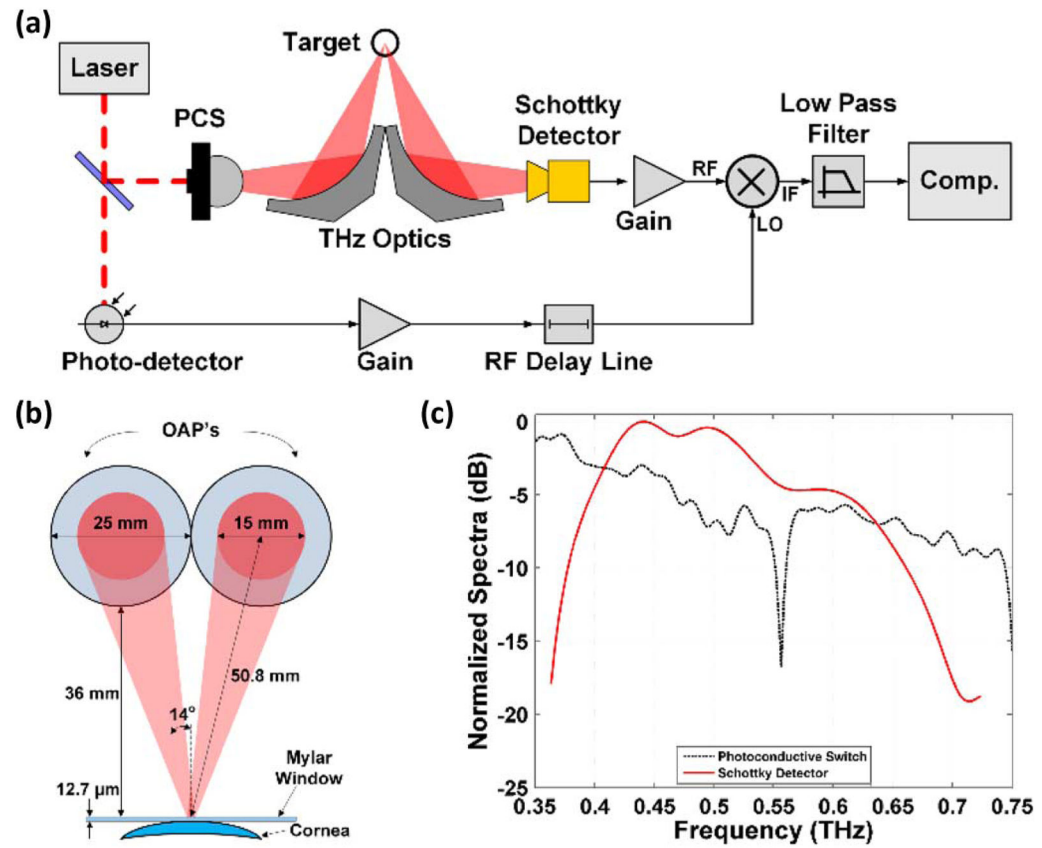
Fig. 1.
Millimeter wave reflectometer. (a) System block diagram. (b) Illumination geometry (c) biasing scheme demonstrating low frequency chopping combined with high frequency FMCW.

Fig. 2.
THz imaging system. (a) System block diagram. (b) Illumination geometry. (c) Photoconductive switch power spectral density and detector spectral responsivity.
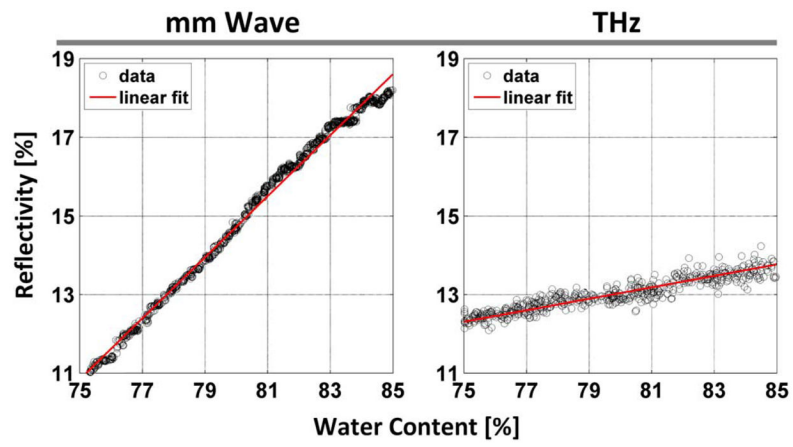
Fig. 3.
Sensitivity analysis of the millimeter wave sensing system (left) and THz imaging system (right). Millimeter wave data from [14] and THz data from [3].
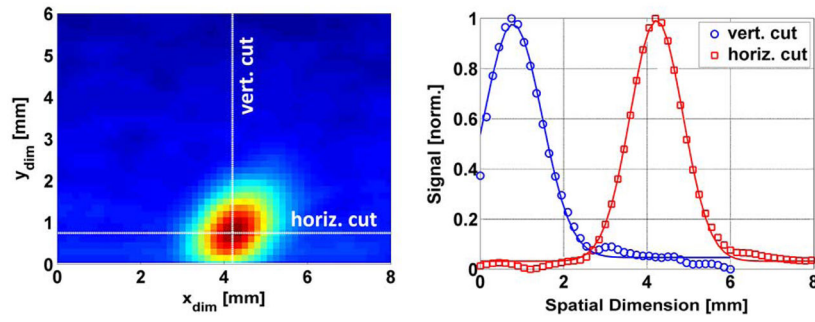
Fig. 4.
Imaging results of corneal geometry phantom (PTFE sphere). (left) THz image of the sphere with the imaging axis parallel to the normal of the sphere apex. (right) Horizontal and vertical cuts through the image superimposed with Gaussian fits.
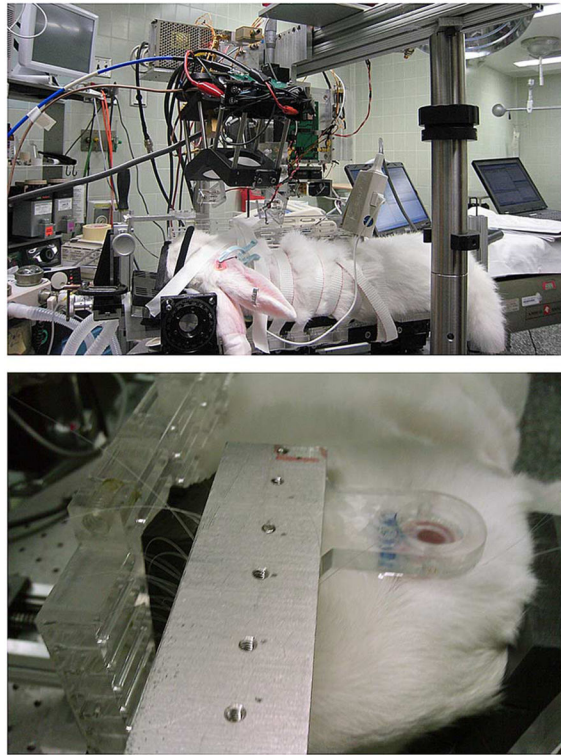
Fig. 5.
Rabbit cornea imaging. (top) Rabbit model placed below the THz and millimeter-wave imaging systems. (bottom) Close-up of rabbit cornea and mylar window.
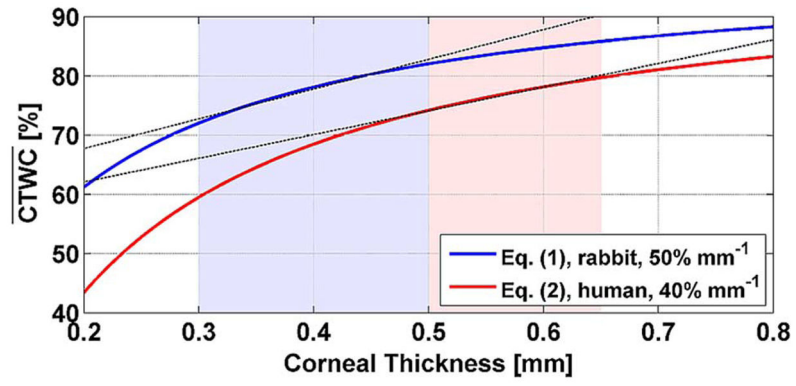
Fig. 6.
Comparison of CCT to CTWC percentage relation for rabbit cornea [see (3)] and human cornea [see (4)].
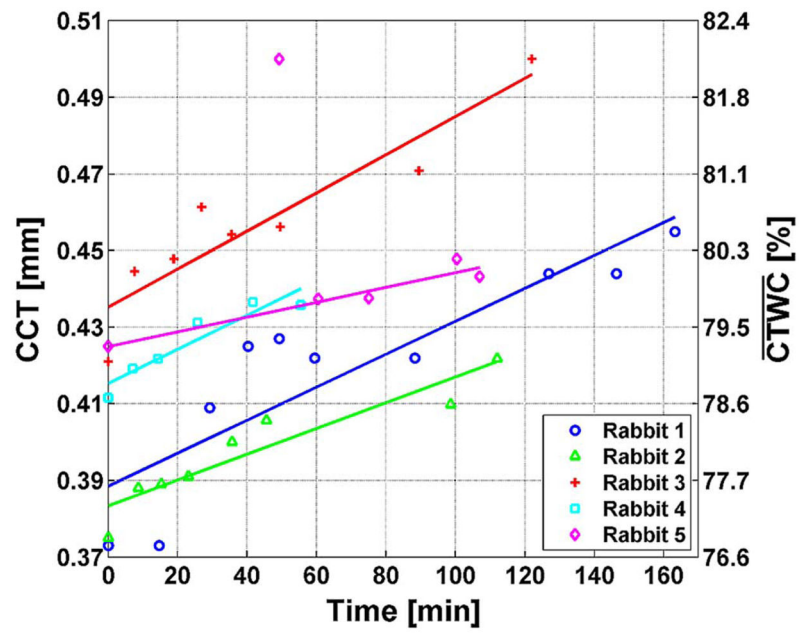
Fig. 7.
CCT measurements for all rabbits in the trial and their associated CTWC levels computed with (3). Rabbit 5 has a large outlier at time 50 min which was not included in the linear fits.
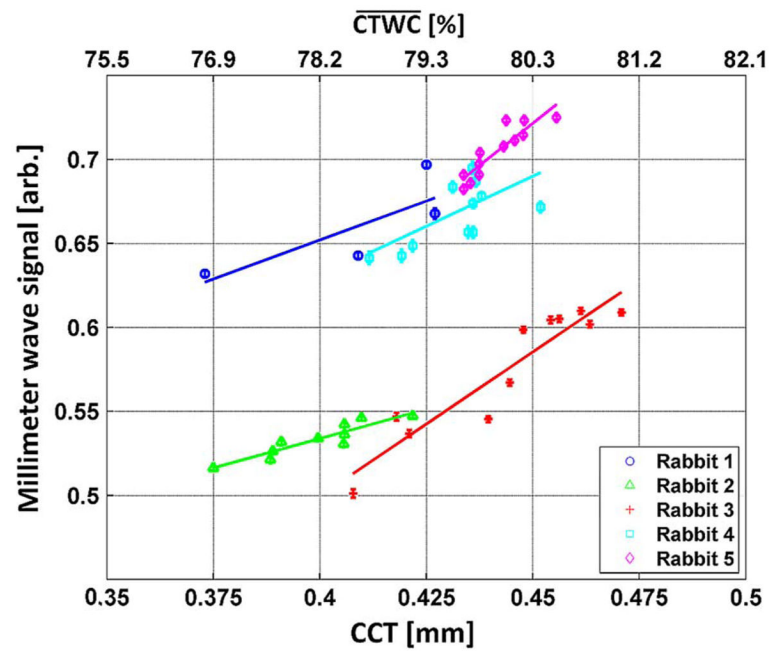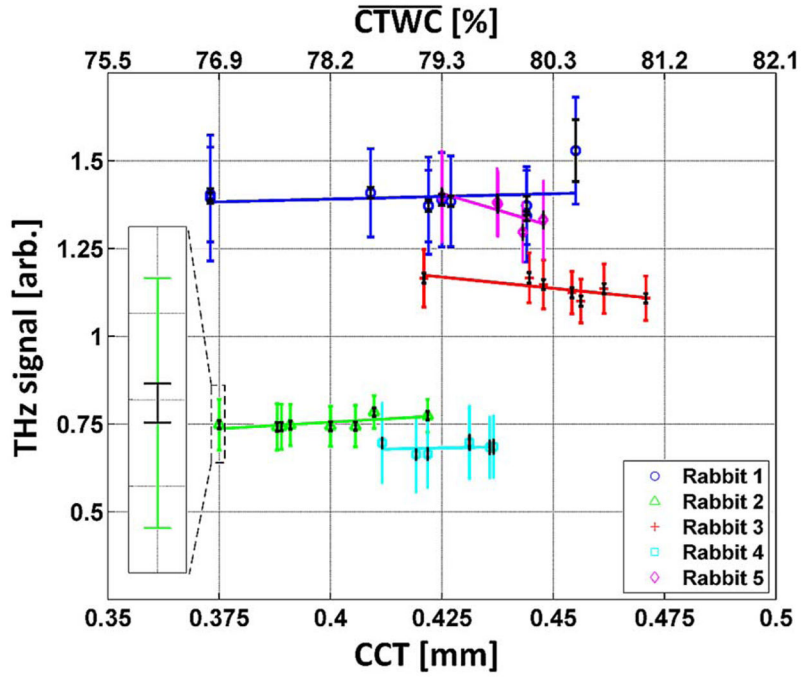
Fig. 8.
100 GHz point measurements plotted against the CCT measurements reflected in the lower *x*-axis. The corresponding CTWC increases predicted by CCT theory are displayed on the top *x*-axis.
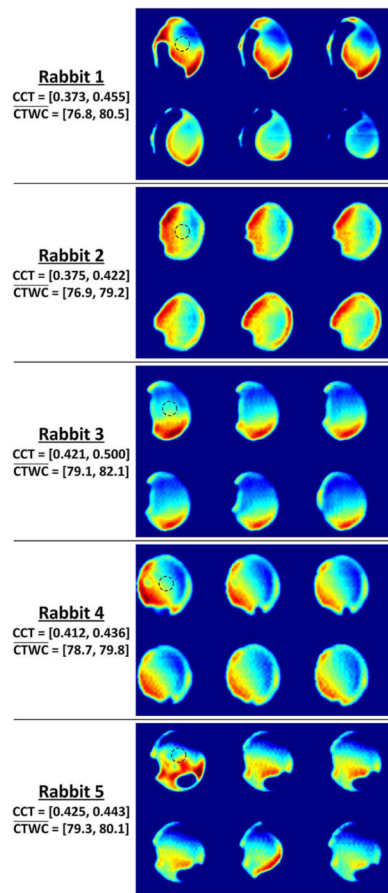
Fig. 9.
Selected THz reflectivity maps of CTWC for all five rabbit models. Each image series is accompanied by its CCT range and computed CTWC levels using (3) Time increases, from left to right and top to bottom for each image series. The dotted circles overlaid on the top left cornea of each image denote the ultrasound probe location.

Fig. 10.
THz reflectivities computed with the indicated region of interest as a function of acquired CCT measurements reflected in the lower *x*-axis. The corresponding CTWC increases predicted by CCT theory are displayed on the top *x*-axis. A zoom-in of the first point in the rabbit 4 series is displayed in the inset demonstrating the difference in variation between estimated system noise and contrast observed in the 5 mm diameter FOV.
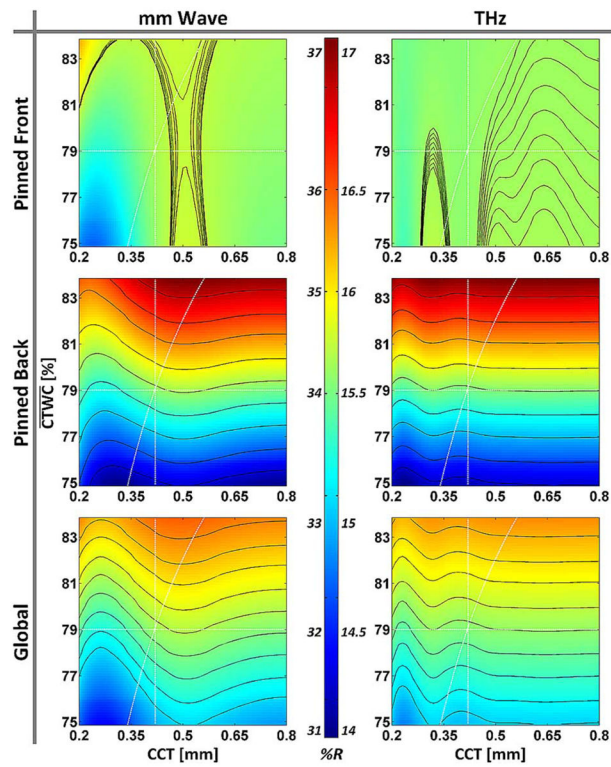
Fig. 11.
Dependence of corneal reflectivity on TWC and thickness computed for the (left column) 100 GHz system and (right column) 525 GHz system for the gradient types (top row) pinned front, (middle row) pinned back, and (bottom row) global. The figures within each row are displayed with a common colormap, with pixel intensities representing reflectivity.
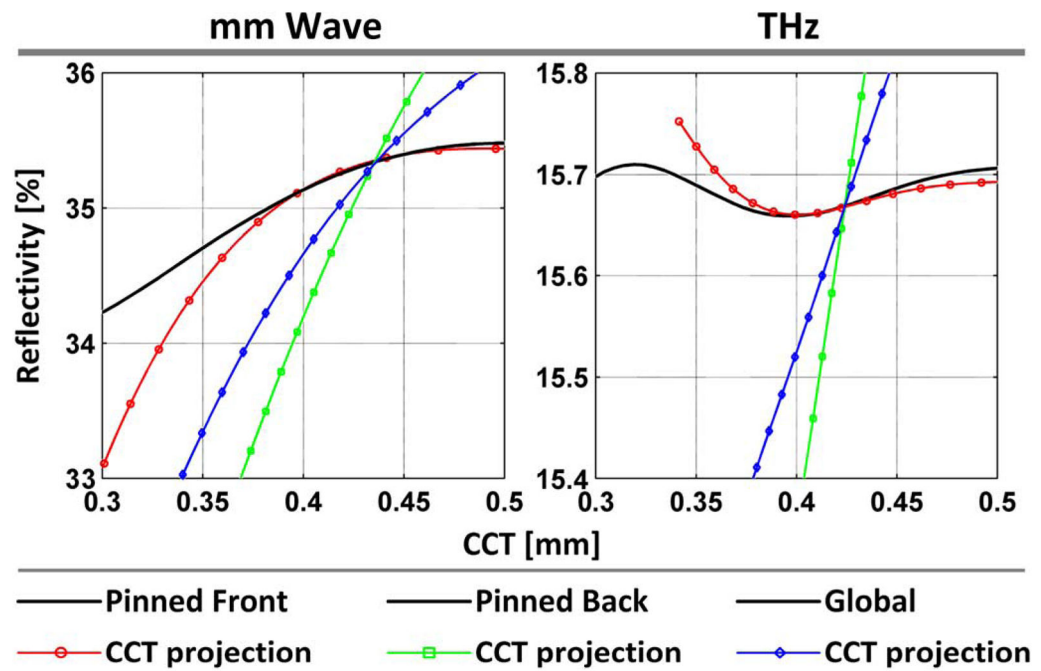
Fig. 12.
Constant CTWC cuts at 79% water by weight with varying distance over the range measured by ultrasound pachymetry. Note that in the case of constant CTWC-varying CCT the three gradient types yield the same behavior which is represented by the solid line.
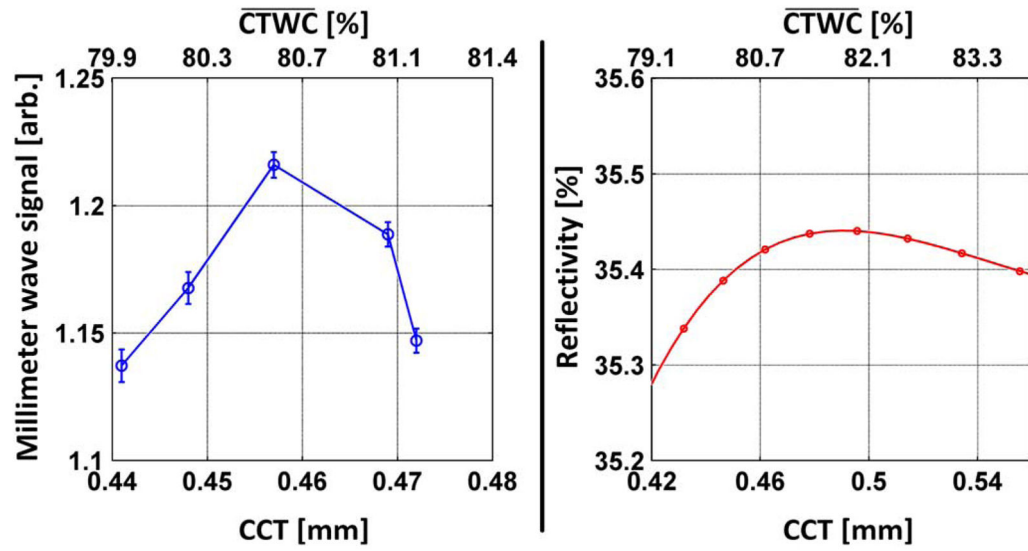
Fig. 13.
Post mortem study. (left) Observed change in reflectivity at 100 GHz per change in CCT.
(right) Predicted change in reflectivity for the pinned front gradient case.

TABLE I

Noise Equivalent Metrics

System	Slope $\left(\frac{dR_s}{dp_w}\right)$ [%/%]	NERD [%]	NE WC [%]
mm Wave	0.7765	0.0587	0.0763
THz	0.1459	0.1204	2.3761

TABLE II

Measured Sensitivities

Rabbit (n)	Measured CCT slope μm/hr	Measured 100 GHz CCT sens. [μm]	Measured THz CCT sens. [μm]
1	25.8	3.27	582.6
2	20.2	3.14	98.2
3	29.9	1.4	−64.2
4	26.7	3.11	476.0
5	11.6	1.29	−34.2